Journal of Power Sources 190 (2009) 485–492

Contents lists available at ScienceDirect

Journal of Power Sources

journal homepage: www.elsevier.com/locate/jpowsour

The impact of thermal conductivity and diffusion rates on water vapor transport through gas diffusion layers

Sergei F. Burlatsky[a,*], Vadim V. Atrazhev[b], Mallika Gummalla[a], Dave A. Condit[a], Fuqiang Liu[a]

[a] United Technologies Research Center, East Hartford, CT 06108, United States
[b] Russian Academy of Science, Institute of Biochemical Physics, Kosygin str. 4, Moscow, 119334, Russia

ARTICLE INFO

Article history:
Received 21 November 2008
Received in revised form
22 December 2008
Accepted 23 December 2008
Available online 14 January 2009

Keywords:
PEM fuel cells
Gas diffusion layer
Thermal conductivity
Water management
Water vapor transport

ABSTRACT

Proper water management in a hydrogen-fueled polymer electrolyte membrane (PEM) fuel cell is critical for performance and durability. A mathematical model has been developed to elucidate the effect of thermal conductivity and water vapor diffusion coefficient in the gas diffusion layers (GDLs). The fraction of product water removed in the vapor phase through the GDL as a function of GDL properties/set of material and component parameters and operating conditions has been calculated. The current model enables identification of conditions wherein condensation occurs in each GDL component. The model predicts the temperature gradient across various components of a PEM fuel cell, providing insight into the overall mechanism of water transport in a given cell design. The water condensation conditions and transport mode in the GDL components depend on the combination of water vapor diffusion coefficients and thermal conductivities of the GDL components. Different types of GDLs and water transport scenarios are defined in this work, based on water condensation in the GDL and fraction of water that the GDL removes through the vapor phase, respectively.

1. Introduction

Optimal water management is important for polymer electrolyte membrane (PEM) fuel cell performance, durability and rapid start-up under frozen conditions. A low rate of water removal from the cathode impedes oxygen transport; while excessive water removal from the electrode may cause electrode and membrane dry-out resulting in low proton conductivity and low apparent exchange current, as well as high losses associated with membrane resistance.

The gas diffusion layer (GDL) is a crucial element that impacts the overall water transport in a PEM fuel cell. Fundamental understanding of liquid water transport in the GDL and associated strategies to keep the bulk volume available for oxygen diffusion is necessary. Experimental determination of capillary pressure as a function of water saturation combined with Darcy's law have been the primary focal points in water management [1–6]. However, recent experimental and modeling results indicate that the transport of liquid water in GDLs is a process of capillary fingering [7–11], which cannot be adequately represented by Darcy's law according to [12]. Liquid water flows through GDL in the form of connected clusters, encountering dead ends due to the presence of varied diameter pores, and eventually percolates through a pathway of the least resistance. On the other hand, Owejan et al. [13] recently found that vapor diffusion is an important mechanism of water removal from the cathode catalyst layer through the GDLs. It is shown that the thermal gradient in the cathode GDL can be sufficient to remove product water in vapor state through the GDL at high current densities [13].

Thermal properties of the GDL and its design are thus very important for high performance and durability [14–17]. Normally, in an operating fuel cell there is 3–5 °C temperature gradient at 1 A cm^{-2} between the catalyst layers and gas channels [18–20]. That corresponds to 8–19% ΔRH at 75 °C cell temperature. The dissipation of the cathode reaction heat relies on GDL effective thermal conductivity, which strongly depends on the anisotropic packing and thermal contact of GDL carbon particles and fibers. Interaction between mass and thermal transport makes favorable water management a challenge. Only a handful of studies have attempted to investigate the thermal impact of GDL on mass transport. Pasaogullari et al. [14] studied the anisotropic heat and water transport in a cathode GDL. Weber and Newman [20] investigated the non-isothermal phenomena and water transport through the membrane. They showed that the temperature gradient within a fuel cell is sufficient to cause a heat-pipe effect where the water is moving from cathode to anode down the temperature gradient. However, these studies did not include a micro-porous layer (MiPL), which is a key component to the GDL (see Fig. 1).

* Corresponding author. Tel.: +1 860 6107211; fax: +1 860 6601045.
E-mail address: BurlatSF@utrc.utc.com (S.F. Burlatsky).

0378-7753/$ – see front matter © 2009 Elsevier B.V. All rights reserved.
doi:10.1016/j.jpowsour.2008.12.131

Nomenclature

D	water vapor diffusion coefficient in porous medium ($cm^2\ s^{-1}$)
D_{eff}	effective water vapor diffusion coefficient in substrate + MiPL composite ($cm^2\ s^{-1}$)
F	Faraday's constant, 96487 ($C\ mol^{-1}$)
ΔH	water latent heat ($J\ g^{-1}$)
i	current density ($A\ cm^{-2}$)
L	thickness (cm)
P_0	saturated water vapor pressure at the WPT coolant temperature ($din\ cm^{-2}$)
$Q^0_{W\to V}$	latent water heat per unit current density ($W\ (A\ cm)^{-2}$)
Q^0_R	specific reaction heat per unit current density ($W\ A^{-1}$)
R	ideal gas constant, 8.7×10^7 erg $(mol\ K)^{-1}$
RH	relative humidity
T	temperature (K)
T_0	WTP coolant temperature (K)
S	specific reaction entropy ($J\ (mol\ K)^{-1}$)
α	fraction of heat that is removed by the cathode-side WTP
η	overpotential (V)
λ	thermal conductivity ($W\ (cm\ K)^{-1}$)
λ_{eff}	effective thermal conductivity of substrate + MiPL composite ($W\ (cm\ K)^{-1}$)
ξ	fraction of water removed through the vapor phase

Subscripts

A	anode
SM	interface between the substrate and MiPL
C	cathode
S	substrate
M	membrane

Although isothermal modeling of MiPLs are available in the literature [21–23], the conclusions from different groups are contradictory. Weber and Newman's modeling results show that the MiPL increases the back-diffusion rate of water from the cathode through the membrane to the anode [22]; however, Passaogullari et al. [21] and Nam and Kaviany [23] showed that the MiPL enhances water removal rate to the cathode gas channel. Recent experimental results from Karan et al. [24] show no statistical impact of MiPL on net water transport across the membrane. Clearly, the role of a MiPL on water transport remains unresolved (see [24] and references therein).

In this work, thermal effects are included in a model based on analysis of a composite GDL (with a MiPL) to elucidate the water transport mechanism in a porous-plate PEM fuel cell. The variations in GDL properties considered are thermal conductivity and water vapor diffusion coefficients. Experimentally determined thermal conductivities are used for quantitative prediction of the transport fluxes. This work also aims to provide insight into the role of MiPL in water transport and a new physical model to clarify the importance of an intermediate porous layer to aid water vapor diffusive transport, as discussed by Owejan et al. [13].

This model accounts for product water vapor transport across the MiPL present in a cathode composite GDL used for either a conventional solid plate or a porous plate system like that described in this work. Porous bipolar plates (as shown in Fig. 1), known as water-transport plates (WTPs) [25–29], were developed by UTC Power. The model does not describe liquid water removal from the substrate layer of the composite GDL, which will be addressed in our future work.

2. Physical model

2.1. Physics assumption

The WTPs perform two main functions in terms of water management. First, when there is excess water, the WTPs provide a removal path for liquid water to prevent flooding. Second, when the gas streams are not saturated, the WTPs provide water for evaporation into the gas channels and humidifies the membrane electrode assembly [27]. The liquid water in the GDL is comprised of water streams flowing from the cathode to WTP and pendant or "stranded" water (as shown in Fig. 1) not connected to the water streams. In order to maximize oxygen transport, it is desirable to remove the major fraction of water in the vapor phase to minimize the fraction of the GDL volume occupied by liquid water streams and to prevent vapor condensation and accumulation of pendant water in the GDL.

The driving force for vapor transport through the GDL is the gradient of water vapor partial pressure (WVPP). The gradient of WVPP is caused by a small temperature difference between the cathode and WTP, resulting in the difference between the equilibrium WVPP in the WTP gas channel and that in the cathode gas pores. Modeling results and experimental data indicate that in the present WTP design, dry inlet gas becomes fully saturated by liquid water coming through the WTP at the gas channel inlet and stays humidified along the entire channel length. For the boundary conditions of this model, we assume that water vapor is in equilibrium with liquid at the cathode/MiPL interface ($x = 1$ in Fig. 1) and the substrate/WTP interface ($x = 0$ in Fig. 1). One would expect that there is zero flux of water from cathode to WTP because at both locations water vapor is equilibrated with liquid water. However, the water vapor concentration is higher at the cathode/MiPL interface than that in WTP because the temperature of the cathode electrode is higher than that of the WTP. That concentration gradient creates the diffusion flux (see Appendix A for more details on thermodynamics of the transport process). We also assume that no condensation or

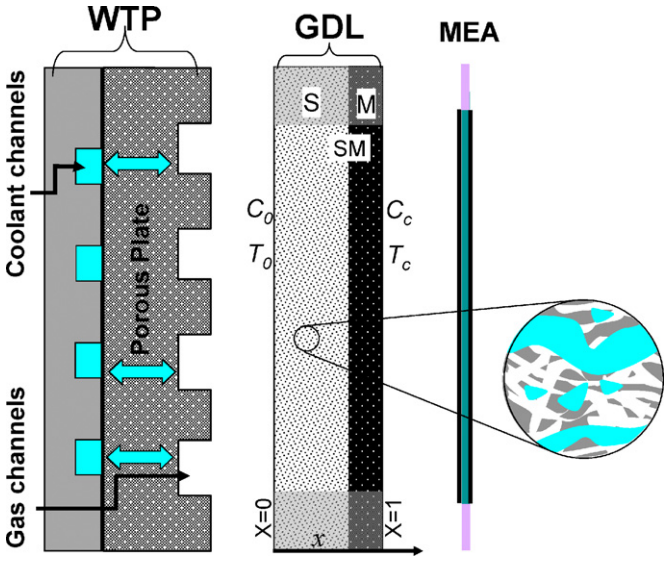

Fig. 1. Schematic of a half fuel cell with water transport plate (WTP). The arrows indicate the flow of liquid water in the WTP. S, M, and SM represent substrate, MiPL, and the interface between substrate and MiPL. Water vapor concentration and temperature at WTP/substrate interface, and, and at MiPL/cathode interface, and, are shown in the figure. Selected area in the substrate is enlarged to show the continuous flow streams and pendant water.

Table 1
Possible Scenarios of water removal through the GDL.

GDL type	Scenario of water dynamics	Condensation in the GDL	Fraction of water removed through the gas phase	Liquid water streams in the GDL	Drops and puddles in the GDL
Type 1	Scenario 1(a)	No condensation under-saturated vapor in the GDL	100%	No	No
	Scenario 2(a)		Less than 100%	Yes[a]	No
Type 2	Scenario 1(a)		100%	No	No
	Scenario 1(b)	Condensation in the substrate Under-saturated vapor in the MiPL	Less than 100%	No	Yes in the substrate
	Scenario 2(b)	Condensation in the substrate Saturated vapor in the MiPL	Less than 100%	Yes	Yes in the substrate

[a] *Note*: The water stream is coming from the MiPL/cathode interface. There is only evaporation in the GDL.

evaporation occurs within the GDL; therefore, there is no source or sink term for the thermal and mass transport equation.

The GDL type defines if condensation and consequent flooding occur in one or more GDL components. The scenario of water transport (see Table 1) defined in this work determines the fraction of water removed through the gas phase. It depends on the combination of water vapor diffusion coefficients, thermal conductivities of GDL components and also on the boundary condition at $x = 0$ and $x = 1$ (see Fig. 1).

2.2. Mathematical formulation

2.2.1. Vapor transport through cathode GDL

In this section, the governing equations of water vapor and thermal transport are introduced. Any in-plan temperature differential is neglected because the in-plan thermal conductivity is one order of magnitude higher than that in through-plan direction [14]. Due to the uniformity of water vapor transport in the PEM fuel cell plan-form, the transport equations can be represented in 1-D, in the through plane of the GDL. The mass and thermal transport governing equations are

$$D\frac{d}{dx}\left(\frac{dC}{dx}\right) = 0 \tag{1}$$

$$\lambda\frac{d}{dx}\left(\frac{dT}{dx}\right) = 0 \tag{2}$$

where x is the through plane direction of the GDL, D the water vapor diffusion coefficient, C the water vapor concentration, and λ is the thermal conductivity. Gas diffusion coefficients in the substrates and MiPLs are corrected by porosity using the Bruggman correlation. Both D and λ are assumed to be constant in each layer.

At the substrate and MiPL interface, fluxes of mass and heat are continuous. This is reflected by mass and heat conservation equations (3) and (4)

$$D_S\frac{C_{SM} - C_0}{L_S} = D_M\frac{C_C - C_{SM}}{L_M} \tag{3}$$

$$\lambda_S\frac{T_{SM} - T_0}{L_S} = \lambda_M\frac{T_C - T_{SM}}{L_M} \tag{4}$$

Solving Eqs. (3) and (4) for vapor concentration at substrate/MiPL, C_{SM}, and for the temperature at substrate/MiPL interface, T_{SM}, we obtain

$$C_{SM} = aC_C + bC_0 \tag{5}$$

$$T_{SM} = cT_c + dT_0 \tag{6}$$

where

$$a = \frac{L_S}{L_S + (D_S/D_M)L_M} \tag{7}$$

$$b = \frac{(D_S/D_M)L_M}{L_S + (D_S/D_M)L_M} \tag{8}$$

$$c = \frac{L_S}{L_S + (\lambda_S/\lambda_M)L_M} \tag{9}$$

$$d = \frac{(\lambda_S/\lambda_M)L_M}{L_S + (\lambda_S/\lambda_M)L_M} \tag{10}$$

Note that $a + b = 1$ and $c + d = 1$. Here L is the thickness of each layer and the subscripts 0, S, M, C, and SM refer to WTP, substrate, MiPL, cathode catalyst layer and substrate/MiPL interface, respectively (see Fig. 1).

2.2.2. Types of GDL and water transport mode

In this section we define different types of GDL as shown in Table 1. The condensation in a PEM fuel cell component occurs when the local water vapor concentration at location x, $C(x)$, is higher than the equilibrium concentration at local temperature, $T(x)$. For common GDL materials, the estimated temperature difference between two GDL interfaces is 1–3 °C at 1 A cm^{-2} (calculated below). Within such a small temperature range, a linear relation between the equilibrium vapor concentration and temperature can be reasonably assumed

$$C^{eq}(T) = A + BT \tag{11}$$

It is assumed that vapor concentration at MiPL/cathode interface, C_C, and vapor concentration at substrate/WTP interface, C_0, are in equilibrium with liquid water according to Eq. (11)

$$C_0(T) = A + BT_0 \tag{12}$$

$$C_C(T) = A + BT_C \tag{13}$$

Substituting C_0 and C_C in Eq. (5) with Eqs. (12) and (13) gives

$$C_{SM} = A + B(aT_C + bT_0) \tag{14}$$

The condition $a = c$, which equals to $b = d$, separates different GDL types. That means water vapor is either condensed or under-saturated at two side of the condition. If $a = c$ or $b = d$, combining with Eq. (6), the above equation becomes

$$C_{SM} = A + BT_{SM} \tag{15}$$

According to Eq. (11), C_{SM}, defined in Eq. (15), equals the equilibrium water vapor concentration. Therefore, water vapor is in equilibrium with liquid water at the substrate/MiPL interface.

To maintain $a = c$ or $b = d$, we must have

$$\frac{D_S}{D_M} = \frac{\lambda_S}{\lambda_M} \tag{16}$$

If the water vapor diffusion rate is larger than the thermal conductivity, i.e.,

$$\frac{D_S}{D_M} > \frac{\lambda_S}{\lambda_M} \tag{17}$$

then

C_{SM} is lower than the equilibrium concentration, C^{eq}_{SM}, determined by Eq. (11).

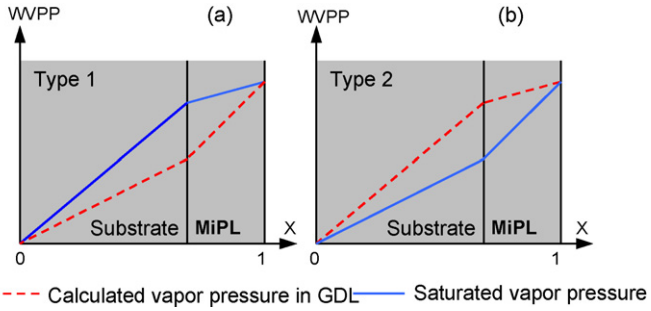

Fig. 2. The WVPP distribution (dashed red line) calculated from the vapor diffusion equations is compared to the WVPP distribution of the saturated vapor (solid blue line). The GDL belongs to Type 1 if the red line is located below the blue line (a) and it belongs to Type 2 otherwise (b). The diffusion equations are solved under the condition that temperature of the cathode/GDL ($x = 1$) interface is higher than that of the GDL/WTP interface ($x = 0$) and the vapor is saturated at these boundaries. (For interpretation of the references to color in this figure legend, the reader is referred to the web version of the article.)

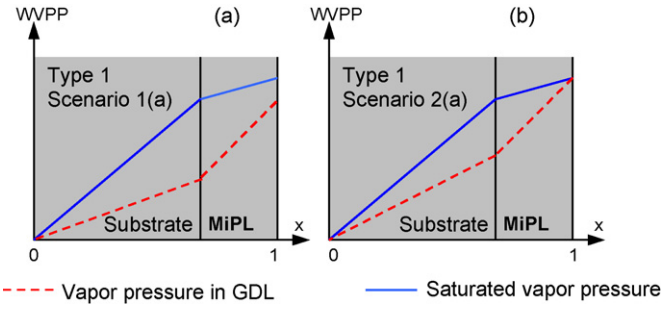

Fig. 3. The WVPP distribution in the GDL of Type 1 is compared to the saturated WVPP distribution. The vapor in the GDL is under-saturated and there is no condensation in any GDL component. In Scenario 1(a), the vapor at the cathode/GDL interface is under-saturated and 100% of water generated in the cathode can be removed through the vapor phase. In Scenario 2(a), the vapor at the cathode/GDL interface is saturated and less than 100% of water generated in the cathode can be removed through the vapor phase.

Thus in this case the water vapor is under-saturated at the interface between the MiPL and substrate. Two types of GDLs are defined based on the water saturation level at the MiPL/substrate interface. The GDL belongs to Type 1 if Eq. (17) holds. Otherwise, the GDL belongs to Type 2. As shown in Fig. 2(a), the GDL belongs to Type 1 if the vapor diffusion equation predicts under-saturated vapor in the GDL. Otherwise, the GDL belongs to Type 2, as shown in Fig. 2(b).

In the above formulation, we assume a saturated water vapor concentration at the MiPL/electrode interface. If the water vapor is under-saturated at this interface, the water vapor concentration in the GDL bulk is even lower than that calculated above. Thus, Eq. (17) is a conservative criterion for not having condensation in the GDL. All the GDLs within Type 1 have under-saturation water vapor in GDL bulk. Type 2 GDLs would have either saturated or under-saturated water vapor in the GDL bulk, as shown in Table 1 and Fig. 4.

2.3. Water transport scenarios

We are not only interested in the water saturation in the GDL, but also the water vapor removal rate in an operating fuel cell. Below we analyze water removal modes through the GDL in an actual fuel cell and classify them into different scenarios. The basis for different scenarios is the fraction of water that the GDL removes through the vapor phase. To calculate this fraction, we compare the water generation rate to the maximum vapor flux through the GDL given that the water vapor is in equilibrium with liquid water at the GDL/WTP interface and that the temperature difference between the WTP and the cathode is fixed.

From Eq. (3), the vapor flux is

$$q_V = \frac{C_C - C_0}{(L_S/D_S) + (L_M/D_M)} \tag{18}$$

Using the ideal gas law to represent the concentration, Eq. (18) can be written as

$$q_V = \frac{1}{R}\frac{(P_C/T_C) - (P_0/T_0)}{(L_S/D_S) + (L_M/D_M)} \tag{19}$$

where P is the water vapor partial pressure. Similar to Section 2.2.2, a linear relation between the water vapor pressure and temperature is assumed

$$P_C = P_0 + (T_C - T_0)\frac{\partial P_0}{\partial T} \tag{20}$$

Then combining Eqs. (19) and (20), eliminating P_C gives

$$q_V = \frac{(T_C - T_0)}{RT_C}\frac{(\partial P_0/\partial T) - (P_0/T_0)}{(L_S/D_S) + (L_M/D_M)} \tag{21}$$

Similar to Eq. (19), the heat flux is

$$q_H = \frac{T_C - T_0}{(L_S/\lambda_S) + (L_M/\lambda_M)} \tag{22}$$

Expressing $(T_C - T_0)$ and substituting Eq. (21) into Eq. (22) gives

$$q_V = \frac{q_H((\lambda_S/D_S) + (\lambda_M/D_M))}{RT_C}\frac{(\partial P_0/\partial T) - (P_0/T_0)}{(L_S/D_S) + (L_M/D_M)} \tag{23}$$

Assume the heat flux through the cathode GDL is proportional to the total heat generated in a fuel cell at specific current density, i, i.e.,

$$q_H(i) = \alpha(Q_R^0 - Q_{W\to V}^0\ \xi)i \tag{24}$$

where ξ is the fraction of water removed in the vapor phase and α is the fraction of heat that is removed from the cathode side (our calculations show that typically, $\alpha \approx 0.25$–0.5). The specific reaction heat Q_R^0 and the latent heat of vaporization $Q_{W\to V}^0$ are calculated as functions of the specific reaction entropy ΔS and overpotential η in the following equations

$$Q_R^0 = T\frac{\Delta S_a}{2F} + T\frac{\Delta S_c}{4F} + \eta \tag{25}$$

$$Q_{W\to V}^0 = \frac{\Delta H \times 18}{2F} \tag{26}$$

Table 2
Criteria determining the scenario of water removal through the substrate.

GDL type	Type 1		Type 2		
Scenario	Scenario 1(a)	Scenario 2(a)	Scenario 1(a)	Scenario 1(b)	Scenario 2(b)
Criteria (17)	True	True	False	False	False
Criteria (27) for the substrate	N/A	N/A	True	False	False
Criteria (27) for the MiPL	N/A	N/A	True	True	False
Criteria (27) for the whole GDL	True	False	N/A	N/A	N/A

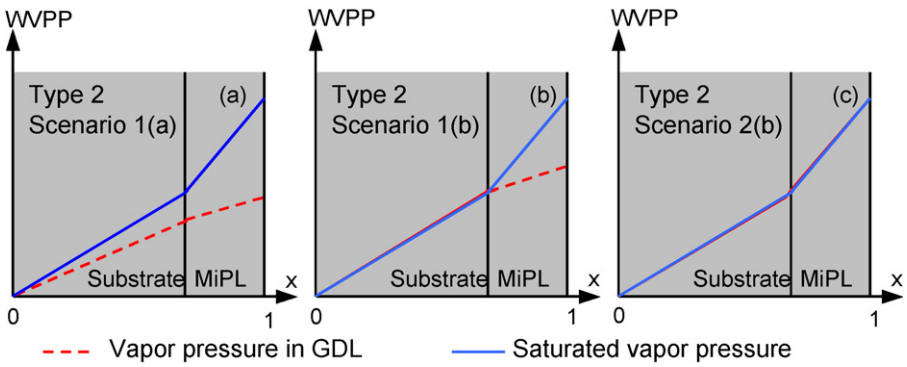

Fig. 4. Actual WVPP distribution is compared to the saturation vapor pressure in the Type 2 GDL. In Scenario 1(a), the actual WVPP is lower than the saturated vapor pressure. In Scenario 1(b), the actual WVPP is equal to the saturated vapor pressure in the substrate. In Scenario 2(b) the actual WVPP is equal to the saturated vapor pressure in the substrate and MiPL.

Here ΔH is the latent heat of vaporization for water. The anode and cathode entropy change, ΔS_a and ΔS_c, are 130 J (mol K)$^{-1}$ and 65 J (mol K)$^{-1}$, respectively [30]. At 1 A cm^{-2} and 0.7 V cell voltage, $Q^0_{W\to V} = 0.21$ W A^{-1} and $Q^0_R = 0.77$ W A^{-1}. The temperature profile within the cathode can thus be calculated using available thermal conductivity data.

The fraction of water removed in the vapor phase, ξ, equals the ratio of the vapor flux to the total water generation rate, which is $i/2F$. The maximum flux that can be removed from the cathode through the vapor phase (calculated in Eq. (23)) in a GDL is higher than the water production rate if

$$\xi = \alpha(Q^0_R - Q^0_{W\to V}\ \xi)\frac{D}{\lambda}\frac{2F}{RT_C}\left(\frac{\partial P_0}{\partial T} - \frac{P_0}{T_0}\right) > 1 \qquad (27)$$

where $(L_s + L_M)/D = (L_s/D_s) + (L_M/D_M)$, $(L_s + L_M)/\lambda = (L_M/\lambda_M) + (L_s/\lambda_s)$. D and λ are the effective vapor diffusion coefficient and thermal conductivity.

The fraction of water removed through the vapor phase (calculated in Eq. (27)) determines the water transport scenario. Different scenarios for Type 1 and 2 GDLs are defined in Table 1. Table 2 summarizes the criteria determining the different scenarios. In the water transport scenarios (see Table 1), 1 corresponds to under-saturated water vapor at the cathode/MiPL interface; otherwise, 2 means saturated vapor at this interface. In the parenthesis, a and b correspond to under-saturated and saturated water vapor at the substrate/MiPL interface, respectively. Therefore, the name of water transport scenario provides vapor saturation details in a GDL.

For Type 1 GDL, we predict Scenario 1(a) if criterion (27) is valid and Scenario 2(a) otherwise. In Scenario 1(a) (Fig. 3a), water vapor in both substrate and MiPL is under-saturated; therefore 100% of the water is removed in vapor phase. In Scenario 2(a) (as shown in Fig. 3b), liquid water streams in the GDL are likely due to possible liquid water transport from the MiPL/cathode interface, where water vapor is in equilibrium with the liquid. However, in this case only water evaporation occurs in the GDL, since the gas is under-saturated in the GDL bulk.

Table 4
Laser flash versus modified substrate method (MTM187) results [33].

	Laser flash thermal conductivity (W (m K)$^{-1}$)	Through-plane thermal conductivity (W (m K)$^{-1}$)
Thin, low Teflon content MiPL only	0.035	0.097
Thin, high Teflon content MiPL only	0.057	0.097
Untreated Toray	1.06	0.798

Scenarios for Type 2 GDL are more complicated (Table 1). The case with lower actual WVPP than the saturated values in the GDL belongs to Scenario 1(a), as indicated in Fig. 4a. If the criterion (27) is not valid for the substrate, but valid for the MiPL, 100% of the generated water is removed in the vapor phase through the MiPL, but some fraction condenses in the substrate. This fraction should be removed through the liquid phase, corresponding to Scenario 1(b) as shown in Fig. 4b. If criterion (27) is not valid for the MiPL, less than 100% of water generated in the cathode is removed in the gas phase. The vapor in the MiPL is saturated, and vapor condenses in the GDL. This corresponds to the Scenario 2(b) in Fig. 4c. Therefore, the main difference between Scenarios 1(b) and 2(b) is the water saturation in the MiPL (in Table 1): the former has under-saturated water vapor in the MiPL and the latter does not.

3. Results and discussion

In order to classify GDLs into the types and water transport scenarios that have been defined, GDL thermal properties are needed. GDL thermal conductivities are currently available through both experimental measurements and estimates in the literature [18,31]. Tables 3 and 4 show the thermal conductivities of substrate, MiPL and different composite combinations, determined by laser flash method [32] and a modified substrate hot plate method [33]. In the laser flash method, the measurement of the thermal diffusivity is usually carried out by rapidly heating one side of a sample using laser energy and measuring the temperature rise on the

Table 3
Laser flash thermal conductivity measurement results [32].

Sample	Thickness, L @ 25 °C (mm)	Bulk density, ρ @ 25 °C (g cm^{-3})	Temperature (°C)	Specific heat, C_p (J (g K)$^{-1}$)	Conductivity, λ (W (m K)$^{-1}$)
Teflon-treated Toray paper	0.19	0.62	65	0.922	2.13
Thick, high Teflon content MiPL + Teflon-treated Toray	0.25	0.61	65	0.870	0.310
Thin, high Teflon content MiPL only	0.045	0.59	65	1.07	0.057
Untreated Toray paper	0.20	0.41	65	0.756	1.06
Thin, low Teflon content MiPL + untreated Toray	0.25	0.50	65	0.862	0.214
Thin, low Teflon content MiPL only	0.070	0.47	65	0.887	0.035

Table 5
Scenarios of water transport for different sets of GDL parameters @ 1 A cm^{-2} (indexes: S, substrate; M, MiPL; α, heat fraction removed through cathode WTP).

MiPL	α	Parameters	Criteria (17)	Criteria (27) for the substrate	Criteria (27) for the MiPL	Scenario
Thin, low Teflon content	0.36	$\lambda_S = 1.06 \times 10^{-2}$ W (cm K)$^{-1}$, $\lambda_M = 0.035 \times 10^{-2}$ W (cm K)$^{-1}$, $\varepsilon_M = 0.78$, $L_M = 25$ μm	False	False	True	1(b)
Thick, low Teflon content	0.22	$\lambda_S = 1.06 \times 10^{-2}$ W (cm K)$^{-1}$ $\lambda_M = 0.035 \times 10^{-2}$ W (cm K)$^{-1}$, $\varepsilon_M = 0.78$, $L_M = 75$ μm	False	False	True	1(b)
Thin, high Teflon content	0.46	$\lambda_S = 0.8 \times 10^{-2}$ W (cm K)$^{-1}$, $\lambda_M = 0.097 \times 10^{-2}$ W (cm K)$^{-1}$, $\varepsilon_M = 0.72$, $L_M = 25$ μm	False	False	True	1(b)
Thick, high Teflon content	0.37	$\lambda_S = 0.8 \times 10^{-2}$ W (cm K)$^{-1}$, $\lambda_M = 0.097 \times 10^{-2}$ W (cm K)$^{-1}$, $\varepsilon_M = 0.72$, $L_M = 75$ μm	False	False	True	1(b)

opposite side. The time that it takes for the heat to travel through the sample and cause the temperature to rise on the rear face can be used to determine the through-plane thermal conductivity. In the other method for substrate conductivity, about 20 samples of substrate are stacked under 690 kPa (100 psi), and the heat flux through the stack is measured with a temperature gradient applied through the stack. The MiPL thermal conductivity was calculated by means of the inverse resistance law from the measured substrate and substrate/MiPL composite thermal conductivity. The measured thermal conductivities of wet-proofed and untreated Toray substrate, Toray/MiPL composites and different MiPLs surprisingly show that the measured MiPL thermal conductivity was about 30% higher than the one calculated by means of the inverse resistance law from the measured substrate and substrate/MiPL composite thermal conductivity. This may be due to the fact that the MiPL penetrates into the substrate. The thermal conductivity results in [33] are about equal for the untreated Toray substrate and 3× and 2× larger than those in [32] for the low and high Teflon content MiPLs, respectively. This may be attributed to considerable thermal contact resistance between the stacked samples. Therefore, the thermal conductivity data measured by the laser flash method were used mostly in this work.

An analysis of the experimental results listed in Table 3 and Table 4 implies Type 2 GDL and Scenario 1(b) (see Table 5) prevailed at 1 A cm^{-2}. That means that condensation is not expected in the MiPL and partial condensation is expected in the substrate as shown in Fig. 4b. Therefore, due to sufficient ΔT, product water is transported through the MiPL only in the vapor phase at $T = 65\,^{\circ}$C. Any water vapor that condenses in the substrate is efficiently removed by wicking to the cathode WTP. This is due to its lower thermal conductivity of the MiPL and therefore a locally high temperature zone is maintained near the cathode. For an untreated Toray substrate thickness of 0.2 mm with a thin and low Teflon content MiPL, the cathode temperature is higher than the WTP temperature by 2.6 °C at 1 A cm^{-2} using the data in Table 3.

The approach provided in this work also enables tuning water transport scenarios by modifying GDL properties. The water transport scenario depends on the water vapor diffusion coefficient, which relies on MiPL porosity as shown in Table 6. The fraction of water removed through the MiPL in the gas phase decreases from 100% to 50% with porosity decreasing from 0.5 to 0.25. If the MiPL porosity is 0.5 then 100% of water is removed by vapor phase (Scenario 1(b)) for both thin and thick MiPLs. The results for thermal conductivity obtained in Table 3 imply that 100% of water is removed through the MiPL in the gas phase even for the thin, low Teflon content MiPL with porosity of 0.25. The experimental results and theoretical models obtained for the current UTC WTP cell design also indicate that the water generated in the cathode @1 A cm^{-2} can be totally removed through the vapor phase. In this case, the water vapor in the GDL can be under-saturated.

Although the model has been developed exclusively from WTP cells, its application is not limited. The work done by Owejan et al. at GM [13] are a suitable experimental verification of this theory in a solid-plate cell. With the same thermal conductivity, cracked and crack-free MiPLs were shown to give the same performance under different humidification levels. This indicates that water vapor diffusion is the primary mode of water removal from the cathode electrode even at high liquid water content (300% outlet RH) [13]. The basis here is the dramatic difference in thermal properties of carbon paper substrates and MiPLs. The thermal conductivity of MiPL is ca. 20× smaller than that of the substrate as shown in Table 3, therefore a localized hot zone is created near the electrode surface, causing an under-saturation environment there.

A primary application for this work is to derive a preferred composite GDL that will maximize performance at high current density. To sustain enough mass transport, the major fraction of water should be removed through the gas phase and condensation in the GDL should be minimized. That means that the desired scenario is Scenario 2(a) and desired GDL type is Type 1 if liquid water and vapor are in equilibrium at the cathode–MiPL interface. On the other hand, for an under-saturated cathode–MiPL interface, drying out of the cathode needs to be prevented and thereby low ionomer resistance has to be sustained. Some fraction of generated water should be removed through the liquid phase as is the case for scenario 1(b) where some water is expected to condense in the substrate where the WTP can evacuate it (liquid water is wicked away and absorbed in the WTP more readily if the substrate is hydrophilic). For high current density with sufficient ΔT across

Table 6
Scenarios of water transport for different MiPL porosity @ 1 A cm^{-2} (indexes: S, substrate; M, MiPL; α, heat fraction removed through cathode WTP).

MiPL	α	Parameters	Criteria (17)	Criteria (27) for the substrate	Criteria (27) for the MiPL	Scenario
Thin, high Teflon content	0.4	$\lambda_S = 0.8 \times 10^{-2}$ W (cm K)$^{-1}$, $\lambda_M = 0.097 \times 10^{-2}$ W (cm K)$^{-1}$, $\varepsilon_M = 0.5$, $L_M = 25$ μm	False	False	True	1(b)
Thick, high Teflon content	0.37	$\lambda_S = 0.8 \times 10^{-2}$ W (cm K)$^{-1}$, $\lambda_M = 0.097 \times 10^{-2}$ W (cm K)$^{-1}$, $\varepsilon_M = 0.5$, $L_M = 75$ μm	False	False	True	1(b)
Thin, low Teflon content	0.36	$\lambda_S = 1.06 \times 10^{-2}$ W (cm K)$^{-1}$, $\lambda_M = 0.035 \times 10^{-2}$ W (cm K)$^{-1}$, $\varepsilon_M = 0.25$, $L_M = 25$ μm	False	False	True	1(b)
Thick, low Teflon content	0.22	$\lambda_S = 1.06 \times 10^{-2}$ W (cm K)$^{-1}$, $\lambda_M = 0.035 \times 10^{-2}$ W (cm K)$^{-1}$, $\varepsilon_M = 0.5$, $L_M = 75$ μm	False	False	True	1(b)
Thick, low Teflon content	0.22	$\lambda_S = 1.06 \times 10^{-2}$ W (cm K)$^{-1}$, $\lambda_M = 0.035 \times 10^{-2}$ W (cm K)$^{-1}$, $\varepsilon_M = 0.25$, $L_M = 75$ μm	False	False	False	2(b)

the GDL, all water for this scenario would be transported through the MiPL in the gas phase. At smaller current density with lower ΔT, a larger fraction of water could be removed through the liquid phase in both the MiPL and substrate. This, however, does not negatively impact performance because the total water flux is lower than that at high current density. Thus, flooding in the MiPL would not be expected.

4. Conclusions

A mathematical model to study water removal modes at the cathode in a porous-plate cell has been developed. The impact of thermal conductivity and diffusion coefficients on water transport in the GDL has been discussed. Assuming saturated vapor at both GDL interfaces, it is concluded that a composite GDL structure (with MiPL) with low thermal conductivity in the vicinity of the cathode–GDL interface helps to sustain under-saturated vapor in the GDL bulk. Water transport (the fraction of water removed by vapor phase and condensation conditions in the GDL components) depends on the combination of water vapor diffusion coefficients and thermal conductivities of the GDL components. Different water removal scenarios were described (Table 1) and the criteria to predict the water removal scenario from GDL properties were provided (Table 2). The desirable fraction of water removed by vapor phase is about 90% for composite GDLs, corresponding to Type 2 and Scenario 1(b) or 2(b), depending on the MiPL thickness and porosity (see Table 6). An analysis of thermal conductivity impact on water transport with different Teflon content in MiPLs predicts that more than 90% of product water (@ 1 A cm^{-2}) is transported through these MiPLs in the vapor phase.

Appendix A

A.1: The driving force of the vapor transport in GDL

At the GDL/WTP interface, water vapor is in balance with liquid water. The water vapor chemical potential at the GDL/WTP interface is equal to the liquid water chemical potential in the WTP. However, the chemical potential of the liquid water in the cathode is higher than the chemical potential of the liquid water in WTP because the temperature of the cathode is higher than the temperature of the WTP. This implies that the water vapor chemical potential in the cathode is higher than the water vapor chemical potential at the GDL/WT interface. The temperature and chemical potential gradients cause the thermo-diffusion and the diffusion fluxes the GDL.

To understand the mechanism of the vapor transport in the liquid-water-free GDL we use a simple cartoon, depicted in Fig. A.1. The cathode and WTP are shown as two vessels, partially filled with liquid water, the GDL is shown as a liquid-water-free pipe between these two vessels. Liquid water is in equilibrium with vapor in both vessels. The temperature of the left hand vessel, T_1, is higher than the temperature of the right hand vessel, T_2, i.e., $T_1 > T_2$. At $P = 1$ atm, the water vapor can be treated as an ideal gas. The chemical potential of 1 mol of ideal gas is

$$\mu_v(P, T) = \mu_v^0(T) + RT\ \ln(P) \tag{A.1}$$

where $P = P/P_0$ is the normalized pressure, p_0 is the partial pressure of gas under the standard condition, $\mu_v^0(T)$ is standard chemical potential of the gas. The concentration of a component of the ideal gas mixture is

$$C = \frac{P}{RT} \tag{A.2}$$

Here P is the partial pressure of a gas component. The chemical potential of the gas component is a function of its partial pressure

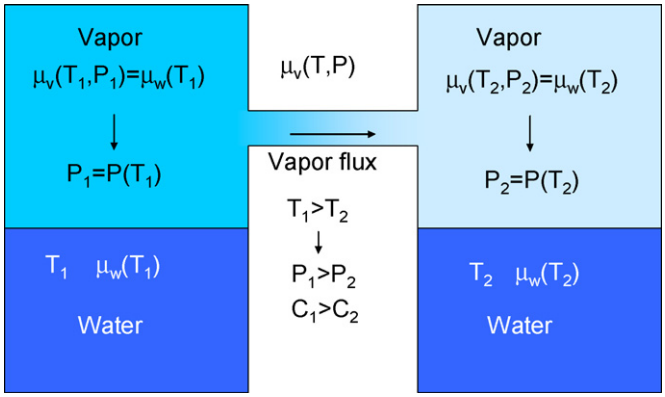

Fig. A.1. In both of the vessels, liquid water is in equilibrium with the vapor and the vapor partial pressure (concentration) is a function of the temperature of the vessel. There is no liquid water in a pipe connecting the vessels so the water vapor concentration and the temperature in the pipe are independent.

P (or concentration C) and of the gas temperature T. The chemical potential of liquid water is a function of the temperature only

$$\mu_w = \mu_w(T) \tag{A.3}$$

In liquid water/water vapor equilibrium system, the water vapor chemical potential is equal to the liquid water chemical potential. From Eqs. (A.1) and (A.3), we obtain the following equation for the saturated vapor pressure in the vessels

$$\mu_w(T) = \mu_v^0(T) + RT\ln(P) \tag{A.4}$$

Solving it with respect to P, we obtain the following dependence of the saturated vapor pressure on temperature

$$P(T) = \exp\left\{\frac{\mu_w(T) - \mu_v^0(T)}{RT}\right\} \tag{A.5}$$

Eq. (A.5) indicates that the vapor chemical potential and pressure in both vessels depend only on vessel temperature. Using the Eq. (A.2) we obtain the following Equation for saturated vapor concentration

$$C(T) = \frac{\exp\{(\mu_w(T) - \mu_v^0(T))/RT\}}{RT} \tag{A.6}$$

Vapor concentration and temperature in the left hand side vessel is higher than that in the right hand side vessel. This results in the chemical potential gradient and in the diffusion flux as shown in following Section.

A.2: Fick's law

If the concentration and temperature gradients in the gas are small, the diffusion flux, j, of one of the gas components, such as water vapor, is a linear function of the gradient of the chemical potential of this component and of the temperature gradient in the gas [34]

$$j = -\alpha \cdot \nabla\mu_i - \beta \cdot \nabla T \tag{A.7}$$

Eqs. (A.4) using (A.2) can be re-written in the form

$$\mu_w(T) = \mu_v^0(T) + RT\ln(C_i RT) \tag{A.8}$$

where the local water vapor chemical potential μ_i is a function of the local water vapor concentration C_i and of the local gas temperature T. The gradient of the chemical potential is a function of the concentration and temperature gradients

$$\nabla\mu = \left(\frac{\partial\mu}{\partial C_i}\right)_T \nabla C_i + \left(\frac{\partial\mu}{\partial T}\right)_C \nabla T \tag{A.9}$$

Substituting (A.9) into (A.7), we obtain the following Equation for the flux

$$j = -\alpha\left(\frac{\partial\mu}{\partial C_i}\right)_T \nabla C_i - \left[\alpha\left(\frac{\partial\mu}{\partial T}\right)_C + \beta\right]\nabla T \tag{A.10}$$

Using the standard definitions of the transport rate coefficients

$$D = \alpha\left(\frac{\partial\mu}{\partial C_i}\right)_T \tag{A.11}$$

$$\frac{k_T D}{T} = \alpha\left(\frac{\partial\mu}{\partial T}\right)_C + \beta \tag{A.12}$$

we finally obtain the following transport rate equation

$$j = -D\left(\nabla C_i + \frac{k_T}{T}\nabla T\right) \tag{A.13}$$

Here k_T is a thermo-diffusion ratio. The diffusion coefficient D depends on the concentrations of all component of the gas and on the temperature. However, if the concentration and temperature gradients are small (as in our case) it can be treated as a constant.

A.3: Kinetic coefficients in the transport equation

The diffusion and thermo-diffusion coefficient cannot be calculated using thermodynamic methods. Kinetic theory [35] provides the following Equations for these coefficients in the gas phase

$$D = \frac{kT}{3P}\left\langle\frac{v}{\sigma_t}\right\rangle \tag{A.14}$$

$$k_T = C_i T\frac{\partial}{\partial T}\ln\left(\frac{\langle v/\sigma_t\rangle}{kT}\right) \tag{A.15}$$

where v is the thermal velocity of the gas component molecule, σ_t is the transport collision cross-section of the gas component molecule (σ_t practically does not depend on the velocity). The mean thermal velocity is a function of the temperature $\langle v\rangle = (kT/m_i)^{1/2}$, where m_i is the molecular weight. Thus, for the thermo-diffusion ratio we obtain the following equation

$$k_T = \frac{C_i}{2} \tag{A.16}$$

Finally, the flux of the gas component is

$$j = DC_i\left[\frac{\nabla C_i}{C_i} - \frac{\nabla T}{2T}\right] \tag{A.17}$$

A.4: Fick's flux versus thermo-diffusion in the GDL

Here we compare the first (diffusion) and second (thermo-diffusion) terms in the right hand side of Eq. (A.17) using the typical GDL conditions in PEM. The first term in the right hand side of Eq. (A.17) is

$$\frac{\nabla C_v}{C_v} \approx \frac{C_C - C_0}{LC_0} \tag{A.18}$$

Here L is the GDL thickness. Using the equation of state of ideal gas, Eq. (A.2), we express the vapor concentration in terms of the partial pressure

$$\frac{\nabla C_v}{C_v} \approx \frac{P_C - P_0}{LP_0} \tag{A.19}$$

Having in mind, that the water vapor is saturated in the cathode and at the cathode/WTP interface, we obtain the following equation for the pressure gradient

$$\frac{P_C - P_0}{LP_0} \approx 2\frac{\partial P_0}{\partial T}\frac{T}{P_0}\frac{\nabla T}{2T} \tag{A.20}$$

Taking advantage of Eq. (A.20), we obtain the following equation for the ratio of the diffusion/thermo-diffusion fluxes

$$\frac{\nabla C_i/C_i}{\nabla T/2T} = 2\frac{\partial P_0}{\partial T}\frac{T}{P} \tag{A.21}$$

At 65 °C,

$$\frac{\nabla C_i/C_i}{\nabla T/2T} = \frac{2\times 10^4\times 340}{25\times 10^4} = 27.2 \tag{A.22}$$

Eqs. (A.21) and (A.22) implies that, under typical PEM operational conditions, the second term (thermo-diffusion) in Eq. (A.17) is much smaller than the first one (diffusion) and that the conventional diffusion equation

$$j = D\nabla C_i \tag{A.23}$$

is applicable to the water vapor transport in GDL.

References

[1] J.D. Fairweather, P. Cheung, J. St-Pierre, D.T. Schwartz, Electrochem. Commun. 9 (2007) 2340–2345.
[2] E.C. Kumbur, K.V. Sharp, M.M. Mench, J. Electrochem. Soc. 154 (2007) B1295–B1304.
[3] E.C. Kumbur, K.V. Sharp, M.M. Mench, J. Electrochem. Soc. 154 (2007) B1305–B1314.
[4] E.C. Kumbur, K.V. Sharp, M.M. Mench, J. Electrochem. Soc. 154 (2007) B1315–B1324.
[5] U. Pasaogullari, C.-Y. Wang, J. Electrochem. Soc. 152 (2005) A380–A390.
[6] U. Pasaogullari, C.Y. Wang, J. Electrochem. Soc. 151 (2004) A399–A406.
[7] V.P. Schulz, J. Becker, A. Wiegmann, P.P. Mukherjee, C.-Y. Wang, J. Electrochem. Soc. 154 (2007) B419–B426.
[8] J. Benziger, J. Nehlsen, D. Blackwell, T. Brennan, J. Itescu, J. Membr. Sci. 261 (2005) 98–106.
[9] P.K. Sinha, C.-Y. Wang, Chem. Eng. Sci. 63 (2008) 1081–1091.
[10] P.K. Sinha, C.-Y. Wang, Electrochim. Acta 52 (2007) 7936–7945.
[11] S. Litster, D. Sinton, N. Djilali, J. Power Sources 154 (2006) 95–105.
[12] N. Djilali, Energy 32 (2007) 269–280.
[13] J.E. Owejan, J.P. Owejan, T.W. Tighe, W. Gu, M. Mathias, Proceedings of FEDSM2007 5th Joint ASME/JSME Fluids Engineering Conference, July 30–August 2, 2007, San Diego, CA, USA, 2007.
[14] U. Pasaogullari, P.P. Mukherjee, C.-Y. Wang, K.S. Chen, J. Electrochem. Soc. 154 (2007) B823–B834.
[15] A.A. Kulikovsky, Electrochem. Commun. 9 (2007) 6–12.
[16] C.J. Bapat, S.T. Thynell, J Power Sources 185 (2008) 428–432.
[17] J.J. Hwang, C.H. Chao, W. Wu, J. Power Sources 163 (2006) 450–459.
[18] M. Khandelwal, M.M. Mench, J. Power Sources 161 (2006) 1106–1115.
[19] H. Ju, H. Meng, C.Y. Wang, Int. J. Heat Mass Transfer 48 (2005) 1303–1315.
[20] A.Z. Weber, J. Newman, J. Electrochem. Soc. 153 (2006) A2205–A2214.
[21] U. Pasaogullari, C.-Y. Wang, K.S. Chen, J. Electrochem. Soc. 152 (2005) A1574–A1582.
[22] A.Z. Weber, J. Newman, J. Electrochem. Soc. 152 (2005) A677–A688.
[23] J.H. Nam, M. Kaviany, Int. J. Heat Mass Transfer 46 (2003) 4595.
[24] K. Karan, H. Atiyeh, A. Phoenix, E. Halliop, J. Pharoah, B. Peppley, Electrochem. Solid-State Lett. 10 (2007) B34–B38.
[25] R. Baldwin, M. Pham, A. Leonida, J. McElroy, T. Nalette, J. Power Sources 29 (1990) 399–412.
[26] C. Reiser, US Patent 5,700,595 (1997).
[27] A.Z. Weber, R.M. Darling, J. Power Sources 168 (2007) 191–199.
[28] D.J. Wheeler, J.S. Yi, R. Fredley, D. Yang, T. Patterson, L. VanDine, J. New Mater. Electrochem. Syst. 4 (2001) 233–238.
[29] J.S. Yi, D. Yang, C. King, AIChE J. 50 (2004) 2594–2603.
[30] M. Wohr, K. Bolwin, W. Schnurnberger, M. Fischer, W. Neubrand, G. Eigenberger, Int. J. Hydrogen Energy 23 (1998) 213–218.
[31] E. Sadeghi, M. Bahrami, N. Djilali, J. Power Sources 179 (2008) 200–208.
[32] D. Condit, S. Burlatsky, Internal results, 2002.
[33] C. King, J. Puhalski, P. Balint, A. Lubag, J.S. Yi, Internal results, 2002.
[34] L.D. Landau, E.M. Lifshits, Hydrodynamics (1986), 323–329.
[35] L.D. Landau, E.M. Lifshits, Physical kinetics (1981), 54–58.